Sky-radiance measurements for ocean-color calibration–validation

Richard Santer and Nadège Martiny

The calibration of an ocean-color sensor or validation of water products is generally based on ground-based extinction measurements from which the aerosol products (optical thickness τ_a and aerosol type) are deduced. Sky-radiance measurements complement the extinction measurements mainly in the aerosol-model characterization. Our basic goal is to promote calibration–validation activities based on the radiative properties of the aerosols rather than their chemical or physical properties. A simple method is proposed (and evaluated) to convert sky radiances measured in the principal plane into atmospheric phase functions P. Indeed τ_a and P are the required inputs to a radiative-transfer code for predicting the top-of-the-atmosphere radiances. The overall error in this prediction is a few percent. This method can operate on a worldwide network on ground-based sun radiometers and then be used to achieve a statistical analysis for validating satellite products. © 2003 Optical Society of America

OCIS codes: 010.4450, 280.0280, 260.5430, 030.5920.

1. Introduction

A. Radiometric Calibration

An accuracy of a few percent is required for the radiometric calibration of ocean-color missions. The calibration protocol usually includes prelaunch radiometric activity as well as onboard checking.[1] For that purpose some ocean-color sensors are equipped with diffuser panels[2] that are supposed to measure solar irradiance on a daily basis [the medium-resolution imaging spectrometer (MERIS), the sea-viewing wide field-of-view sensor (SeaWiFS)]. Nevertheless it is difficult to separate the degradation of the sensor calibration from a change in panel reflectance. The lunar calibration[3] has been used as well for the SeaWiFS sensor to indicate variations in the panel characteristics. This technique consists of assuming that the Moon is a diffuse reflector whose surface remains unchanged. The sensor points at the Moon each month to evaluate the temporal degradation of its sensitivity in each channel.[4] For MERIS two panels are used: One is deployed occasionally (to avoid degradation in the space environment) to cross check the panel routinely used. The cross-calibration between sensors is also often used to check the validity of the sensors' sensitivity. For example, a marine observation satellite (MOS) was recalibrated by using the SeaWiFS data,[5] and polarization and directionality of the Earth's reflectances (POLDER) were cross-calibrated with an ocean color and temperature scanner (OCTS). A current and secure means of calibration to provide good ocean-color products is vicarious calibration[6] for which we need an accurate description of the optical properties of both the atmosphere and the ocean body.

B. Validation of Atmospheric Corrections

For ocean-color satellite missions the atmospheric-correction task is quite challenging, depending on the radiometric performance of the instruments (calibration, linearity) and the assumptions used (modeling of the signal, suitability of the aerosol standard models) in the algorithms. The first approach to validating the atmospheric corrections is to validate the aerosol model (the aerosol optical thickness and type) used to perform them. For SeaWiFS the atmospheric products are compared with the AERONET products[7] as well as Simbad, Prede, and Micro Tops measurements. The main output of the atmospheric-correction routine is the water-leaving radiance L_w. A relevant validation of the algo-

The authors are with Laboratoire Inter-diciplinaire des Sciences de l'Environment, Etudes des systèmes Litoraux et Cotier, Unité Mixe de Recherche 8013, Université du Littoral Côte d'Opale, 32 avenue Foch, 62930 Wimereux, France (e-mail for R. Santer, santer@mren2.univ-littoral.fr; for N. Martiny, martiny@mren2.univ-littoral.fr).

Received 28 January 2002; revised manuscript received 23 August 2002.

0003-6935/03/060896-12$15.00/0

rithms is measurement of *in situ* L_w at the time of the satellite overpass for comparison with ocean-color products, but as a practical point of view this is not easy and the representation of the *in situ* measurements is questionable. In the open ocean one can believe that a measurement from a boat on a water spot of the magnitude of 1 m in size can represent a pixel as large as 1 km from space but over coastal waters, this assumption is no longer reasonable. Over coastal environments we have to find another relevant way to validate the atmospheric-correction schemes.

C. Simple Formulation of the Signal

The top-of-the-atmosphere radiance L_{TOA} expressed as

$$L_{\mathrm{TOA}} = L_{\mathrm{atm}} + tL_w \qquad (1)$$

requires knowledge of the transmittance t. Equation (1) is used directly for vicarious calibration and is easily inverted for obtaining L_w. We want a good characterization of the atmospheric functions L_{atm} and t from atmospheric *in situ* measurements. If it is possible to measure the diffuse transmittance from the surface through flux measurements, it is not possible to measure L_{atm} from the ground. We need then to estimate the atmospheric functions from computations by using a radiative-transfer code (RTC). Even if accurate modeling of the signal is supposed to manage a RTC dealing with multiple scattering and polarization, a simplified formulation of the signal will help analyze the key parameters. Following Gordon and Wang,[8] we define the diffuse atmospheric transmittance t as

$$t(\theta, \lambda) = \exp\left\{ -\left[\frac{\tau_r(\lambda)}{2} + \tau_{o3}(\lambda)\right]\frac{1}{\mu}\right\} t_a(\theta, \lambda), \qquad (2)$$

where μ is the cosine of the zenith angle; τ_r, τ_{o3}, and τ_a are the Rayleigh, ozone, and aerosol optical thicknesses, respectively; and t_a is the diffuse aerosol transmittance expressed as

$$t_a(\theta, \lambda) = \exp\left\{ -\frac{[1 - F_a(\mu, \lambda)]\tau_a(\lambda)}{\mu}\right\}, \qquad (3)$$

with

$$F_a(\mu, \lambda) = \frac{1}{4\pi}\int_0^{2\pi}\int_0^1 Pa(\Theta, \lambda)\mathrm{d}\mu\mathrm{d}\phi, \qquad (4)$$

where $P_a(\Theta)$ is the aerosol phase function times the aerosol single-scattering albedo ${\omega_0}^a$. We also need to compute the atmospheric path radiance L_{atm}. In the primary scattering approximation we have

$${L_{\mathrm{atm}}}^{(1)}(\mu, \varphi) = \frac{\tau_{\mathrm{tot}}P(\Theta)}{4\mu}\left\{1 + \frac{P(\chi)}{P(\Theta)}[r(\theta_s) + r(\theta_v)]\right\}. \qquad (5)$$

In Eq. (5) we have first the intrinsic atmospheric path radiance ${L_{\mathrm{atm}}}^{(1)}$ proportional to τ_{tot}, the total optical thickness, and to $P(\Theta)$, the total phase function times the total single-scattering albedo ω_0. Then we add the coupling term between the forward scattering and the Fresnel reflection, which invokes $P(\chi)$ as well as the Fresnel coefficients for the solar and view zenith angles $r(\theta_s)$ and $r(\theta_v)$. According to Eqs. (1)–(5), τ_a and ${\omega_0}^a P_a(\Theta)$ are necessary to describe the aerosol contribution. In what follows we note the ${\omega_0}^a P_a(\Theta)$ product as $P_a(\Theta)$ in order to lighten the text. The same parameters are also used to correct for the multiple scattering.

Through Eqs. (2)–(5) different scattering angles Θ are involved for which knowledge of the phase function is required. First, we need to know $P(\Theta)$ at Θ, which corresponds to the Sun–target–sensor geometry. $P(\chi)$ is a corrective term and χ corresponds to the forward-scattering angle between the reflected solar beam and the view direction (or between the direct solar beam and the direction reflected toward the sensor). In Eq. (4) $P(\Theta)$ is integrated in the forward scattering.

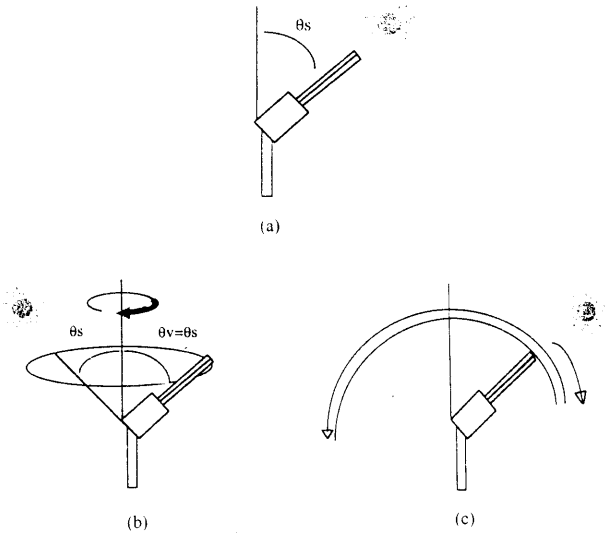

Fig. 1. Three different measurement protocols for the automatic CIMEL E-318: (a) SUN procedure, (b) ALM, (c) PPL.

D. Ground-Based Measurements

The ground-based measurements that we used are performed with a CIMEL E-318 radiometer dedicated specifically to the optical characterization of the aerosols. This instrument is equipped with four filters of at least 1020, 865, 670, and 440 nm. Between the filter wheel and the electronic part of the radiometer, there are two collimators, one for sky-radiance measurements (the SKY collimator) and the other for both sky measurements and aiming directly at the Sun (the SUN collimator). There are several procedures for measurements used by the CIMEL: the SUN procedure for extinction measurements, the almucantar (ALM), and the principal plane (PPL) procedures for diffusion sky measurements. For the SUN procedure [see Fig. 1(a)] the CIMEL uses the SUN collimator and aims at the Sun so as to take

extinction measurements for each filter. For the ALM procedure [see Fig. 1(b)], the CIMEL aims at the Sun and takes measurements at the Sun zenith angle with its SKY collimator with a complete azimuthal rotation (75 view azimuthal angles of the measurements). For the PPL procedure [see Fig. 1(c)] the CIMEL aims at the Sun and takes measurements in the vertical plane that contains the Sun for 40 view zenith angles. The SKY measurements, both ALM and PPL, are taken for the same four filters. All the CIMEL data that we use are from the AERONET network. The data are free and available at http://aeronet.gsfc.nasa.gov. Subsection 1.E is dedicated to a description of the CIMEL data and associated products.

E. Computation of the Aerosol Phase Function from Extinction Measurements

A traditional approach is to define the aerosol model and then use the Mie theory to compute $P_a(\Theta)$. Extinction measurements give accurate estimates of the aerosol optical thickness. The dynamic angstrom coefficients are defined as the spectral dependency of the aerosol optical thickness following

$$\alpha(\lambda_1, \lambda_2) = \frac{\ln[\tau_a(\lambda_1)/\tau_a(\lambda_2)]}{\ln(\lambda_1/\lambda_2)}. \quad (6)$$

We can also determine the mean coefficient by fitting the curve $\ln[\tau_a(\lambda)] = f[\ln(\lambda)]$. In that case the mean value of α is the slope of the regression. If only extinction measurements are available, α can be used to define the simplest approximation for the aerosol distribution $n(r)$ in the atmosphere:

$$n(r) = \frac{dN}{dr} = Cr^{\upsilon}, \quad (7)$$

where υ is the Junge parameter directly related to the angstrom coefficient by

$$\upsilon = \alpha - 3. \quad (8)$$

To point out the performance of this aerosol distribution, we use extinction measurements of the CIMEL sunphotometer (τ_a, α) and the associated Junge size distribution for the aerosol model as the input of the RTC to simulate PPL downward radiances. The code used for the simulations is based on the successive order of scattering.[9] The code of the successive order of scattering can take into account the multiple scattering and polarization in the atmosphere as well as the reflection of the rough surface. On 20 July 1999 over the Venice site the atmosphere was stable with a significant quantity of aerosols: $\tau_a = 0.4$ at 865 nm with $\alpha = -0.80$. The simulations of the PPL radiances were done at $\theta_s = 34°$ in the morning and for three aerosol refractive indexes ($m = 1.33, 1.45, 1.55$). Figure 2(a) shows that the forward peak of the measured radiances is not retrieved, whereas in a first approximation the Junge power law is easily used to retrieve the signal for other scattering angles. If we look at more details [see Fig. 2(b)], retrieval of the measured radiances depends a lot on the refractive index: If a bad aerosol refractive index is selected, errors can go as high as 25%. In conclusion the simple Junge size distribution is too crude for retrieval of the PPL radiance measurements.

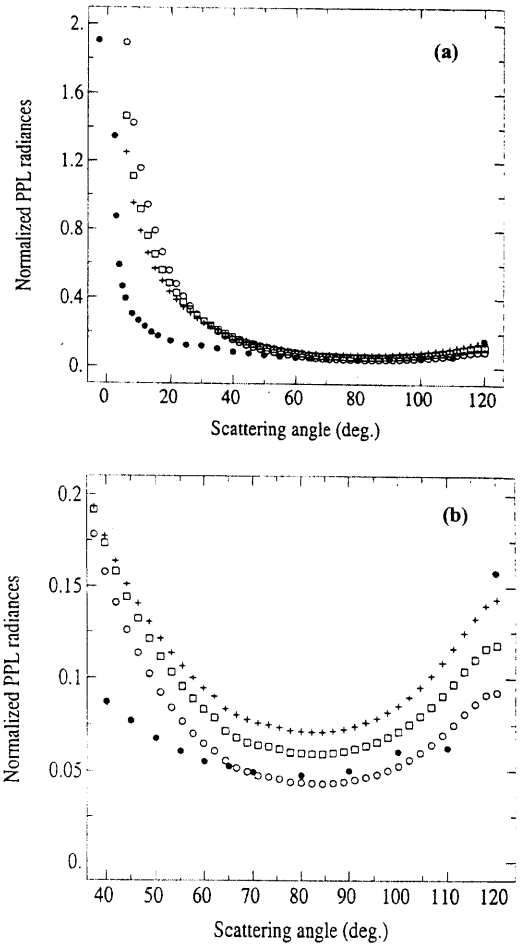

Fig. 2. (a) ●, PPL radiances at $\lambda = 865$ nm measured by CIMEL 20 July 1999 over the Venice site for $\theta_s = 34°$. We also simulated the sky radiances by using a Junge size distribution ($\upsilon = -3.$ with three aerosol refractive indexes: ○, 1.33; □, 1.45; +, 1.55, absorption. (b) Zoom in the backward scattering.

F. Computation of the Aerosol Phase Function from Sky-Radiance Measurements

Abundant literature has been devoted to inver techniques applied to extinction measurements and sky radiances to derive the aerosol model (see, fo example, Santer and Herman,[10] Nakajima *et al.*, and Wang and Gordon[12]). Dubovik and King[13] al proposed an algorithm applied routinely to the CI MEL data. For example, we used the aerosol phas function and the aerosol single-scattering albedo de rived from the Dubovik and King method to retriev the CIMEL PPL measurements of 31 August 199 over the Venice site (45°18′N, 12°30E). Simulation of the PPL radiances were performed for $\theta_s = 54°$ the afternoon with an aerosol optical thickness 0.028. In Fig. 3 we present the relative differenc

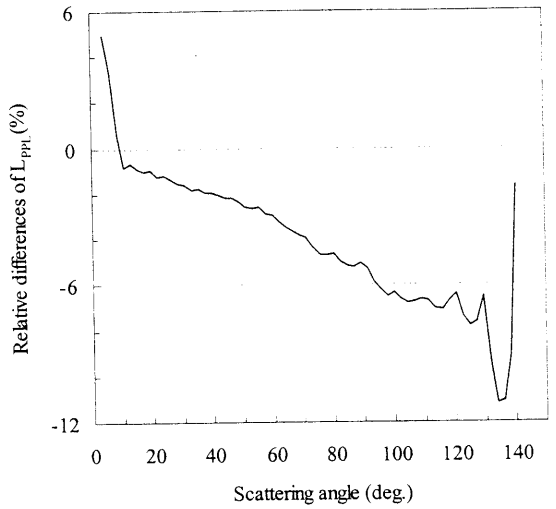

Fig. 3. Simulations of PPL radiances measured by CIMEL 31 July 1999 over the Venice site by using aerosol parameters derived with the Dubovik and King method: aerosol phase function and $\omega_0{}^a = 0.89$. $\theta_s = 54°$. $\lambda = 865$ nm. The relative differences between simulations and measurements versus scattering angle are shown.

between the PPL measurements and the corresponding simulations. Retrieval of the PPL measurements is always better than 5% in the forward direction. This is coherent with the fact that Dubovik and King derived the phase function from the ALM protocol, specifically dedicated to the study of large particles that scatter mainly in forward directions. In the backward direction the discrepancies still remain higher than 6%, increasing to 11% at 135° of the scattering angle even during this clear day. We did tests on a few other cases, and the results were always the same. Actually the method of Dubovik and King (as well as the other existing methods) was dedicated more to the microphysics of the aerosols than to the derivation of equivalent optical parameters dedicated to the retrieval of L_{atm} and t, which is crucial in the derivation process of L_w [see Eq. (1)]. This is especially true when research is done on the satellite geometry where retrieving the backward-scattering signal is most important.

2. Derivation of the Phase Function from Sky-Radiance Measurements

The originality of our study relies on the estimation of $P_a(\Theta)$ by using sky-radiance measurements without any assumptions about the aerosol model. The principle is straightforward: (i) We have to correct for multiple scattering. (ii) The primary scattering we get is simply proportional to P. This simple scheme was described by Devaux *et al.*[14] to derive the aerosol single-scattering albedo with the angular normalization of the phase function. Gordon and Zhang[6] first proposed deriving P from sky-radiance measurements in the same context as predicting the TOA satellite radiances. They used an iterative method with the following steps: (i) An aerosol optical thickness, an aerosol phase function P_a, and a single-scattering albedo $\omega_0{}^a$ were used to compute downward sky radiances. (ii) Discrepancies between simulations and measurements were analyzed in the primary approximation to derive a new $\omega_0{}^a P_a$. (iii) The process was iterated to retrieve the measured sky radiances. What we propose here is quite similar to some modifications: (i) We first noticed that use of a Junge size distribution as a first guess for the aerosol model may create simulated radiances quite far from the values that we want to retrieve (see Fig. 2). (ii) According to Devaux *et al.*,[14] the corrective factor f defined as

$$f = \left[\frac{L^{(1)}}{L}\right]_{\text{theo}} \approx \left[\frac{L^{(1)}}{L}\right]_{\text{mes}}, \tag{9}$$

where $L^{(1)}$ is the primary scattering in the atmosphere and L is the total radiance, was not very sensitive to the aerosol model. So our scheme is based on an iterative estimate of f with as a first guess the aerosol parameters given by the CIMEL extinction measurements (τ_a, α) and the associated Junge size distribution. Simulated $L^{(1)}$ and L are obtained with the successive order of scattering RTC. The boundary conditions, for measurements collected at sea, correspond to the Fresnel reflection associated with a wave-slope distribution given by the Cox and Muck model. The wind speed is the input to this surface contribution.

We simulated f at 865 nm at two solar zenith angles ($\theta_s = 30°$ and 60°) for three Shettle and Fenn[15] aerosol models, maritime (M90), tropospheric (T90), and urban (U90), for a relative humidity of 90%. An aerosol optical thickness of 0.127 corresponds to 23-km visibility. The wind speed is 7.2 m/s. In parallel we simulated f for a Junge slope ν of -3.2, -4.5, and -4.4 corresponding, respectively, to the M90, T90, and U90 spectral dependency. The discrepancies (see Fig. 4) are the most important for the maritime model, especially at limb views, where they can reach 0.8% for $\theta_s = 30°$ and 1.3% for $\theta_s = 60°$. In case of tropospheric and urban models the most important discrepancies are observed for $\theta_v = \theta_s$. They are not significant because they never exceed 0.4% for $\theta_s = 30°$ and 0.8% for $\theta_s = 60°$. Even if the Junge law does not allow retrieval of the CIMEL PPL measurements (see Fig. 2), we can use it for a first estimate of f.

Once the measured PPL radiances are corrected for the multiple-scattering effects, we can use the primary scattering formulation for a homogeneous atmosphere to derive P:

$$P(\Theta) = 4L^{(1)} \exp\left(\frac{\tau_{\text{tot}}}{\mu_v}\right)\left\{1 - \exp\left[-\tau_{\text{tot}}\left(\frac{1}{\mu_s} - \frac{1}{\mu_v}\right)\right]\right\}^{-1} \times \left(\frac{\mu_s}{\mu_v - \mu_s}\right)^{-1}, \tag{10}$$

where μ_v and μ_s are the cosines of the view and solar zenith angles, respectively. If we have sky-radiance measurements in the same band as SeaWiFS, we

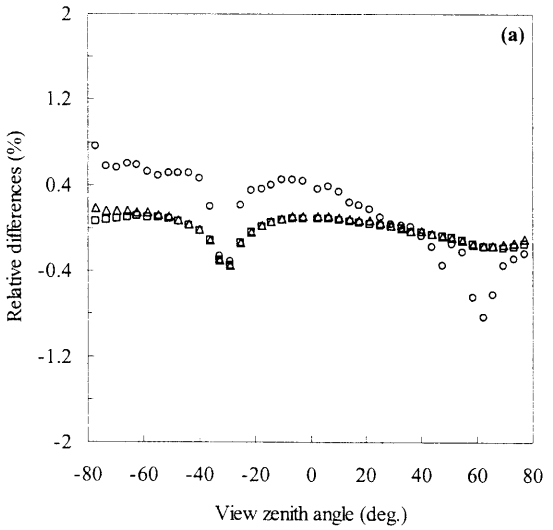

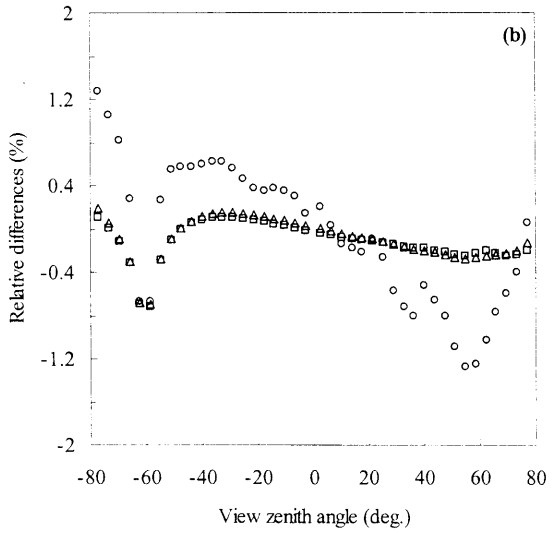

Fig. 4. Simulations of corrective factors f for three Shettle and Fenn aerosol models, M90, T90, and U90, and the three associated Junge slopes ν, -3.2, -4.5, and -4.4. $\tau_a = 0.127$. $\lambda = 865$ nm. Relative differences are plotted between f for each model: ○, M90; □, T90; △, U90. Two θ_s are selected: (a) $\theta_s = 30°$, (b) $\theta_s = 60°$.

have suitable input for the RTC. This is the case for SeaWiFS bands 2, 6, and 8. If we work with another SeaWiFS band, we can derive the aerosol phase function times the aerosol single-scattering albedo P_a in the CIMEL band quite directly from

$$P(\Theta) = \frac{\tau_a P_a(\Theta) + \tau_r P_r(\Theta)}{\tau_a + \tau_r}, \qquad (11)$$

because P_a can be interpolated between two CIMEL bands at any SeaWiFS band as well as τ_a.

A. Correction for Multiple Scattering: Sensitivity Analysis

The corrective factor f is primarily estimated from the extinction measurements and associated aerosol optical thickness. The behavior of f with the aerosol optical thickness is easily predictable: The f parameter is very sensitive to turbidity, and the angular dependence indicates that the primary scattering dominates in the forward scattering. Because the calibration is at 0.5% of accuracy in irradiances, we do not believe that f is significantly affected by the inaccuracy of τ_a.

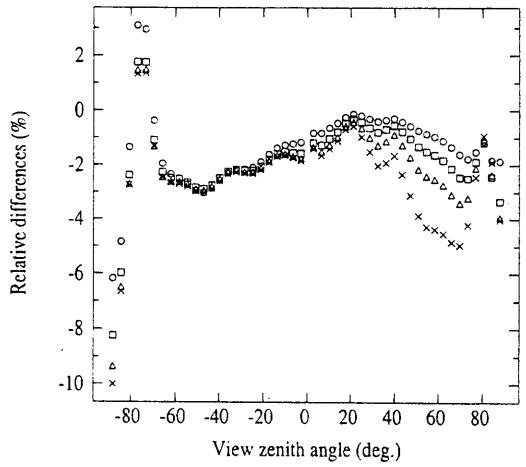

Fig. 5. Relative differences between f simulated for two Junge slopes (-3.5 and -4.0) at four wavelengths: ○, 443 nm; □, 560 nm; △, 670 nm; +, 865 nm.

At order 0, f is computed with the Junge size distribution. We selected two Junge slopes (-3.5 and -4.0) to test the sensitivity of α only (see Fig. 5). We set τ_a to 0.2 for four wavelengths (1020, 865, 670, and 443 nm), which corresponds to clear atmospheric conditions in the blue and the turbid atmosphere conditions in the IR. Globally the error is more important at 865 nm than at 443 nm. Indeed the relative abundance of the aerosols is less important in the blue than in the red. In the worse case the error can reach 5% in the backward direction. In the forward peak we are closer to the primary scattering as the particles get larger.

The sensitivity of f to the real part of the aerosol refractive index m_r is given as follows: 1.33 corresponding to maritime particles and 1.45 corresponding to continental ones. There is no absorption and the simulations are done for four wavelengths (see Fig. 6). In the worse case at 443 nm the errors can reach 3.5%. At 865 nm the errors can go as high as 2%. The same computations with $m = 1.45$ and 1.55 give maximum errors of 6% at 443 nm and 3% at 865 nm. In conclusion, f is not very sensitive to the real part of the aerosol refractive index assumed, whatever the wavelength.

The imaginary part of the aerosol refractive index k represents the absorption of the aerosols. It is directly related to the aerosol single-scattering albedo $\omega_0{}^a$. We tested the sensitivity of f to k, assuming that $m_r = 1.45$. The simulations were done at four wavelengths. Two k's were selected, 0.0 for the case of nonabsorbent aerosols and -0.020 for the case of absorbent aerosols, to cover all the possibilities for the values of absorption in a coastal environment. The value $k = -0.020$ corresponds approximately to

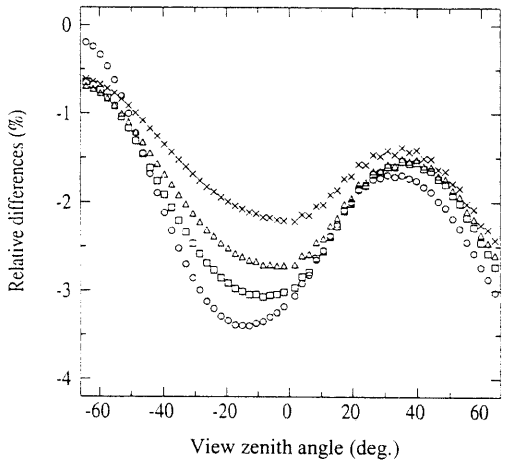

Fig. 6. Same as Fig. 5 but with a Junge slope of −4 and two aerosol refractive indexes (1.33 and 1.45) with no imaginary part.

a $\omega_0{}^a$ of 0.8 according to the 6S code, an update of the 5S code.[16] In Fig. 7 the relative differences between f derived for $k = 0.0$ and $k = -0.020$ are plotted for four wavelengths. Aerosol absorption reduces the multiple scattering more effectively in the backscattering. The difference between this and the previous study is that the discrepancies between the nonabsorbent and the absorbent case are much more important. At 443 nm the discrepancies can reach 13%, and at 865 nm they can reach 11%. The choice of k is then much more crucial than the choice of m_r in the derivation of f.

However, all the errors above are secondary because the Junge model is used only to start the iterative process. In the definition of f the total radiance is computed by using the rough ocean as a boundary condition. Standard values of the water reflectances are assumed to be dark in the computation of the sky radiances. They are negligible in the red and in the IR and residual in the visible, which allows for the use of standard values. Nevertheless we need to include the Fresnel reflection. This term is triggered by the wind speed W and the model of the associated wave-slope distribution. Computations were conducted at 865 nm for the T90 model, with a visibility of 23 km, and for three solar angles of 30°, 60°, and 75°. Four wind speeds were considered and relative discrepancies from a case without Fresnel reflection are reported in Fig. 8. Simulations were done on the principal plane. As expected the influence of the Fresnel reflection is smaller in the forward peak. Toward the backscattering we definitively must correct for the Fresnel reflection. Doing so, with the meteorological wind-speed value (known within 1 m/s), determination of f will be achieved with an accuracy of better than 1%.

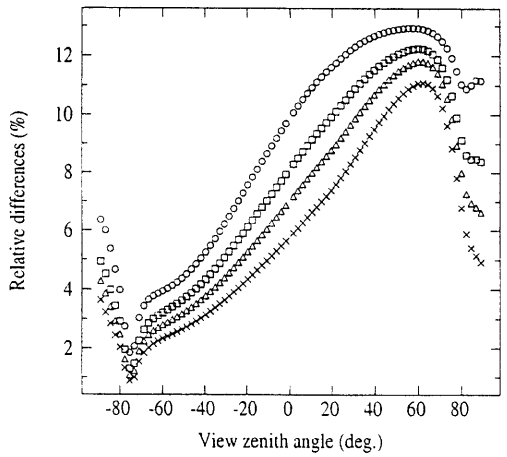

Fig. 7. Same as Fig. 6 but with $m = 1.45$ and two imaginary parts: 0 and −0.02.

B. Iteration of f

To iterate the computation of f, we used the first estimate of P_a. The RTC that we used requires the expansion of P_a into Legendre polynomials following

$$P_a(\mu) = \sum_{l=0}^{\infty} \beta_l p_l(\mu), \tag{12}$$

with

$$\beta_l = \frac{2l+1}{2} \int_{-1}^{1} P_a(\mu) p_l(\mu) d\mu. \tag{13}$$

The integral in Eq. (13) supposes that P_a is defined between $\Theta = 0$ to 180°. In the forward-scattering peak it is reasonable to say that we can measure to as great as 3°. P_a is extrapolated on a log scale toward $\Theta = 0°$. In backscattering, measurements on the PPL correspond to $\Theta = \theta_s + \theta_v$. All the RTC computations were made assuming a plane-parallel atmosphere and the estimate of f is reasonable to as great as $\theta_s = \theta_v = 75°$. As the scattering angle covering the PPL measurements goes to as great as 150°, we need to extrapolate P_a until 180° is reached. We chose, to extrapolate up to 180°, the phase function computed for the Junge Power Law associates to the Ängstrom coefficient measured by CIMEL. In Fig. 9 we illustrate the extrapolation of P_a for the T90 model. P_a is quite sensitive to the aerosol refractive index in the backward scattering; here we use $m = 1.45$. Nevertheless, as discussed by Devaux *et al.*,[14] the effect of this angular extrapolation on P_a is quite negligible in determining $\omega_0{}^a$. In Fig. 9 we demonstrate the ability to retrieve P_a with a Legendre polynomial expansion even if we do not know the actual phase function beyond $\Theta = 150°$. In the following we use $m = 1.45$ for the extrapolation of P_a. We will apply a classical truncature to P_a when the forward scattering is too high in order to limit the length of the Legendre expansion.

At order 0, f is computed with a Junge power law, $m = 1.45$ and $\omega_0{}^a = 1.0$. At order n, f is computed by using the phase function at order $n - 1$. We applied this process for three Shettle and Fenn aerosol models (see Fig. 10). For the M90 model four iterations were required because of the rainbow, but for the T90 and U90 models only two and three iterations, re-

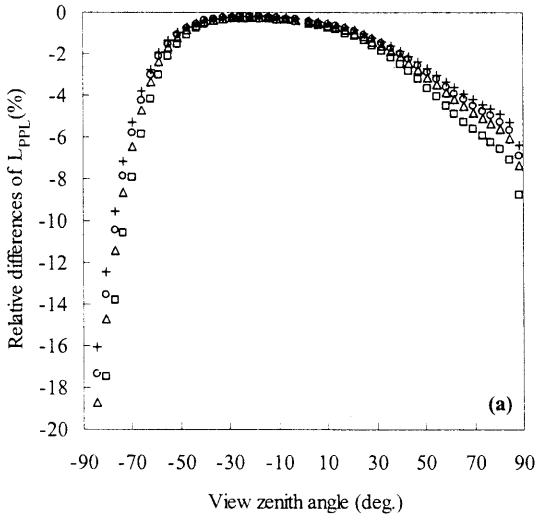

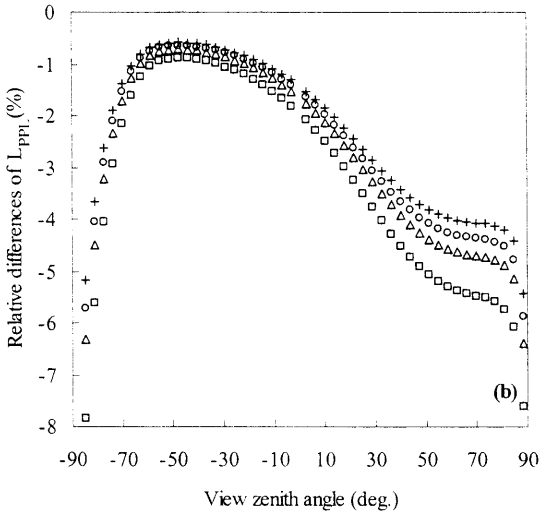

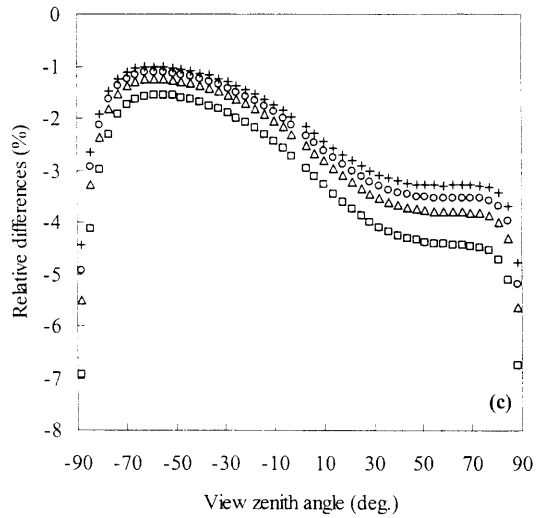

Fig. 8. Influence of the rough sea surface in simulations of PPL radiances at 865 nm. Four wind speeds are considered: □, 2 m/s; △, 5 m/s; ○, 7 m/s; +, 10 m/s. Relative differences between PPL radiances simulated for a flat surface and PPL radiances simulated for a rough surface are represented versus the view zenith angle for three solar zenith angles: (a) 30°, (b) 60°, (c) 75°. The model for the simulation is the T90 model. Visibility is 23 km.

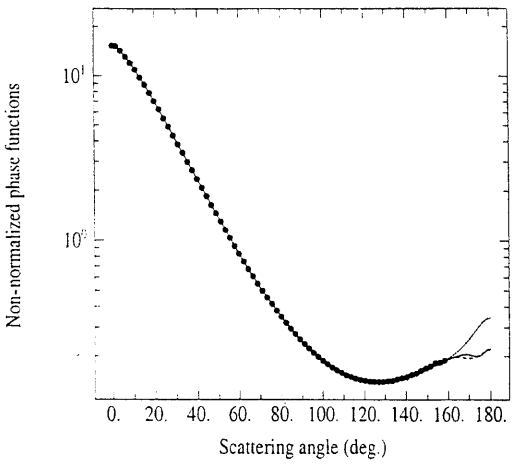

Fig. 9. Extrapolation of the non-normalized aerosol phase function inverted for the T90 Shettle and Fenn model to as great as 180° by using the corresponding Junge-size distribution with three aerosol refractive indexes (solid curve, 1.33; dashed curve, 1.45; microdashed curve, 1.55).

spectively, were needed to achieve the convergence of f. As a practical point of view the geometry of the satellite observation corresponds to a scattering angle Θ. According to Eq. (5), we mainly need to estimate $P(\Theta)$ and we stop the iteration process when $f(\Theta)$ converges within 0.5%. For the complementary scattering angle χ needed to take into account the coupling between scattering and the Fresnel reflection, the convergence obtained at Θ will also ensure good retrieval of $P(\chi)$.

3. Computation of Top-of-the-Atmosphere Radiance

A. Phase Function to Top-of-the-Atmosphere Radiance

We now have the necessary inputs to compute the TOA radiances. Some assumptions have been made regarding the RTC inputs. First, we neglected the polarization of the aerosols, and, second, we mixed the aerosols and the particles homogeneously in order to apply Eq. (10). These two assumptions are applied both ways: in a backward mode on the measured downward radiances to derive P_a and in a forward mode to compute the TOA radiances from P_a. So, we will counterbalance the induced error on P_a in the backward mode in the forward mode to predict the TOA radiances. The error is maximum in the blue. We computed the exact TOA radiances at 443 nm in a plane perpendicular to the principal plane for two solar-zenith angles (30° and 60°). The aerosol models are M90, T90, and U90 for a visibility of 23 km [τ_a(550 nm) = 0.24]. The aerosols are distributed vertically with an exponential decrease with the altitude z for a scale height, H_a = 3 km. For the molecules (Rayleigh) H_r = 8 km. We also derived the phase functions from simulations, with the same aerosol models, from the downward radiances in the principal plane for a solar zenith angle of 75°. The accuracy of the TOA retrievals depends slightly on the aerosol model and is always better than 1% (see

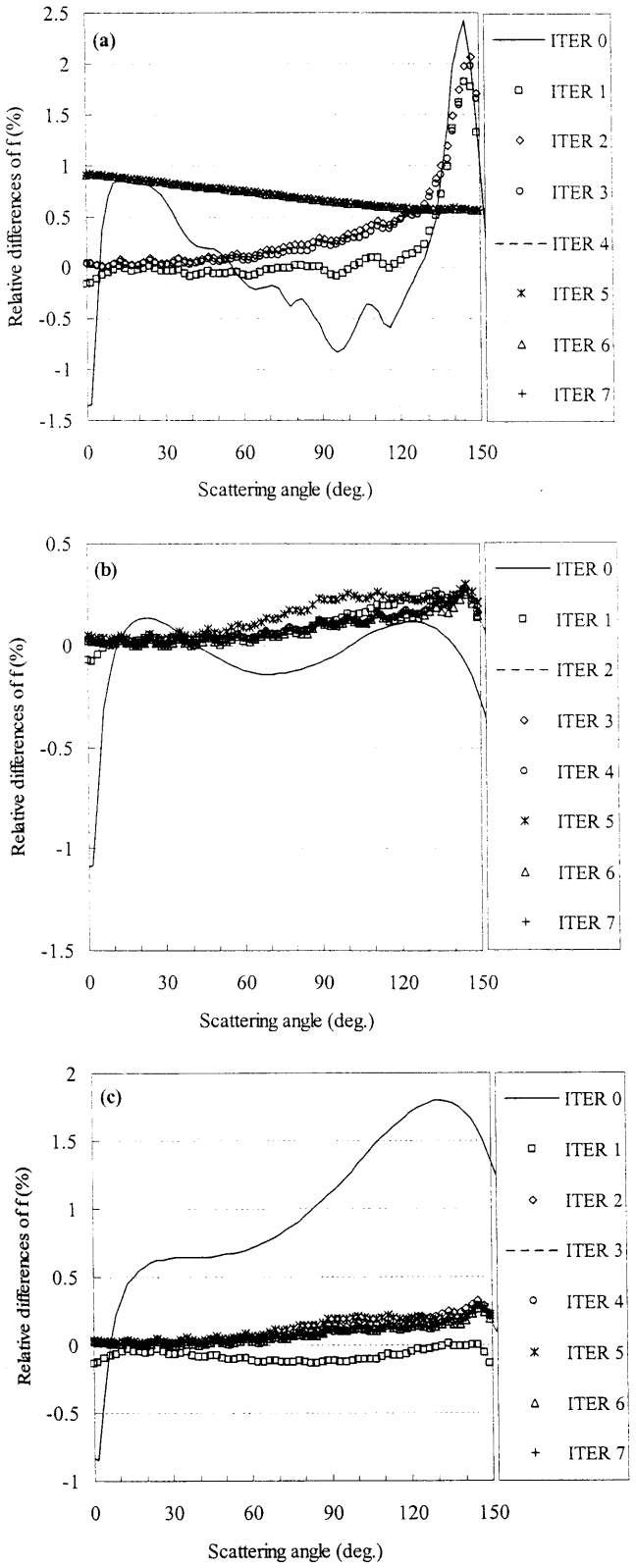

Fig. 10. Convergence of the f parameter: (a) M90 model, (b) T90 model, (c) U90 model.

Fig. 11). This error becomes negligible in the near IR because the primary scattering is predominant, which cancels the residual effects of the vertical distribution as well as a possible bias due to the aerosol polarization effect on the radiances for higher scattering orders.

B. Uncertainties due to Radiometric Calibration of the Ground-Based Radiometer

The other input to the RTC is the water-leaving radiance L_w, at least at short wavelengths. In a vicarious satellite calibration we suppose that L_w is well known, and for atmospheric corrections our first guess for L_w is through the current ocean-color products. However, L_w has been determined so far with sufficient accuracy for P_a to be determined from the downward radiances. Generally, the aerosol optical thickness is easily determined. The irradiance calibration of a sun radiometer is conducted with the classical Langley–Bougueur plots. With an autotracking system there are enough clear and stable days to achieve accurate calibration.

Our experience[17] indicates that we can achieve a radiometric calibration within 0.5% which results in the same accuracy on the aerosol optical thickness. Because the aerosol path radiance is proportional to the aerosol optical thickness, the overall effect on the TOA radiances will be negligible. The main uncertainty will result from uncertainties in the radiance calibration of the ground-based radiometer. In Fig. 12 we point out that errors of 2% and 4% on the initial downward PPL radiances implies an error of the magnitude of 2% and 4% on the TOA radiances, whatever the wavelength and the solar zenith angle. In the limb views the error is amplified a little, but this does not matter in the SeaWiFS geometry for which solar zenith angles are often not higher than 60°. The M90 model and a visibility of 23 km have been used for these simulations. The radiance calibration was realized in the laboratory by using integrating spheres. The accuracy was better than 4% in the IR and of a magnitude of 4% at 443 nm. In conclusion the most important uncertainty in the proposed method lies in the uncertainty of the calibration of the CIMEL radiances.

C. Phase Function from the Measured Radiance

What are the practical considerations that we must deal with? The ideal case for obtaining simultaneously a space measurement at a scattering angle Θ and ground-based measurements at the same angle never occurs. A satellite overpass near noon, such as for SeaWiFS, will give small solar zenith angles most of the time. Then it is not possible from the ground to have access to the backscattering region at the time of the overpass to match the satellite geometry. So, we need to collect sky measurements at low solar elevations to cover the largest scattering-angle domain. The phase function that we will derive from these measurements should be stable with time for as long as the time of the satellite overpass. The temporal stability of the aerosols can be checked by the optical thicknesses that should be stable or at least should depict the same angstrom coefficient as an indicator of the stability of the aerosol model. Also during the day it is recommended that P_a be

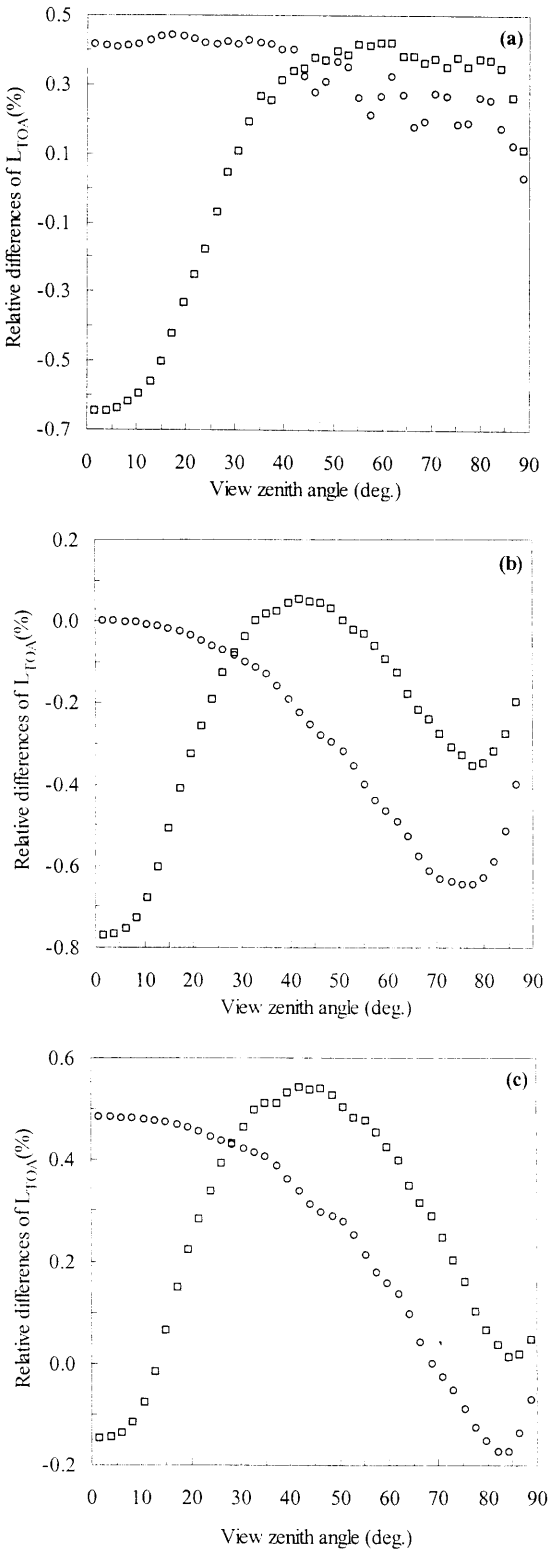

Fig. 11. Accuracy of the TOA radiance retrieval at 443 nm perpendicular to the principal plane for two solar-zenith angles: □, θ_s = 30°; ○, θ_s = 60°. The aerosol models are three Shettle and Fenn models: (a) M90, (b) T90, (c) U90. Visibility is 23 km [$\tau_a(550)$ = 0.24].

compared at least on the same scattering-angle domain. For example, we derived the non-normalized phase functions ($\omega_0{}^a P_a$ product, still noted P_a) at 3 h

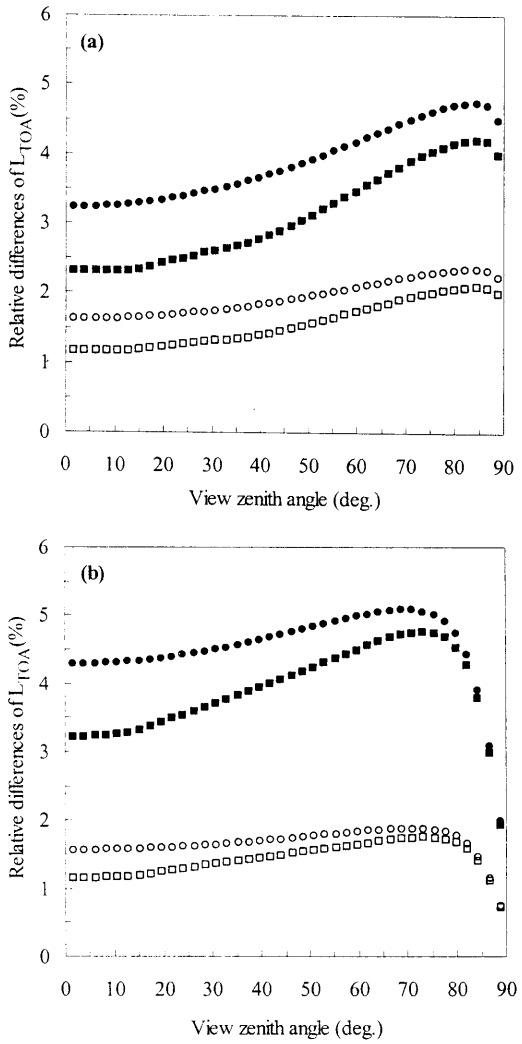

Fig. 12. Influence of the uncertainties on the CIMEL calibration on the TOA radiance retrieval at (a) 865 nm and (b) 443 nm. Relative differences of the TOA radiances when there is an error in the radiance calibration of, open symbols, 2%; and solid symbols, 4%, for two solar-zenith angles: squares, θ_s = 30°; circles, θ_s = 60°. Visibility is 23 km in both cases.

for 8 June 2000 over the Venice site from measured PPL radiances at 865 nm. We selected a day with clear and stable atmospheric conditions. As shown [see Fig. 13(a)] the measured radiances create no instability events. The aerosol optical thicknesses were low and steady during the day, as was the spectral dependency of the aerosols (see Table 1), which implies a stability of the inverted phase functions [see Fig. 13(b)]. On the other hand, in Fig. 13(b) we point out that we have to work on really stable days because small instabilities, often not detectable with radiance measurements, can induce artifacts such as those observed for the phase function, as represented by circles (P_a derived for θ_s = 53°). In that case we will not use P_a as an input of the RTC. The scattering angles covering the phase function go as high as 140° for the PPL protocol done for θ_s = 72°, but a bad value at 130° implies a bad restitution in the backscattering due to the Gauss interpolation.

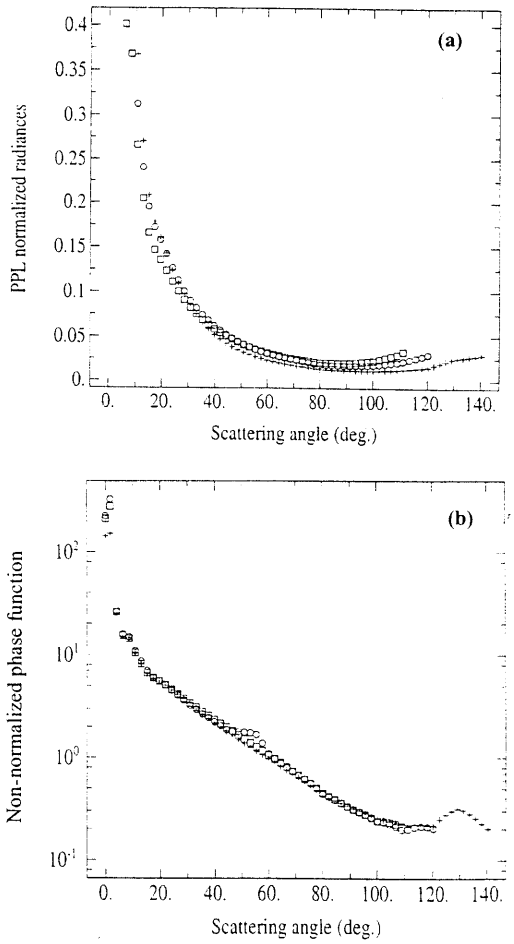

Fig. 13. Typical aerosol phase functions derived from radiance measurements collected in Venice 8 June 2000: (a) Solar-zenith angles of the PPL protocols: ○, 53°; □, 42°; +, 72°. (b) The corresponding inverted aerosol phase functions are not normalized.

Table 1. Aerosol Parameters Used for Inversion of Phase Functions 8 June 2000 over the Venice Site

θ_s (deg)	H (decimal)	τ_a (865)	α (443/865)
53	7.18	0.063	−1.47
42	8.18	0.092	−1.50
72	16.95	0.073	−1.53

We investigated the stability of P_a on 20 July 1999 over the Venice site for 2 hours: early in the morning (5:50 a.m.) and late in the afternoon (4:55 p.m.) and two wavelengths (865 and 670 nm). Fig. 14 are the relative differences between the non-normalized phase functions in the morning and the afternoon versus the scattering angle. Except in the forward direction the discrepancies never exceed 1.5%, at 865 or 670 nm. This shows the stability of the day and in that case we can derive P_a in the morning for computation of the TOA radiances around noon.

The geometrical conditions of SeaWiFS offer mostly large scattering angles. To illustrate this, we represented the histogram of the scattering angles of

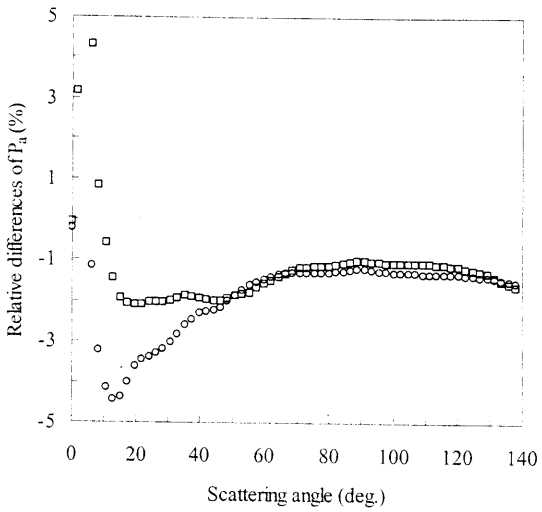

Fig. 14. Relative differences between a phase function derived in the morning (5:50 a.m.) and a phase function derived in the afternoon (4:55 p.m.) 20 June 1999 over the Venice site. The derivations are for two wavelengths: □, 865 nm; ○, 670 nm.

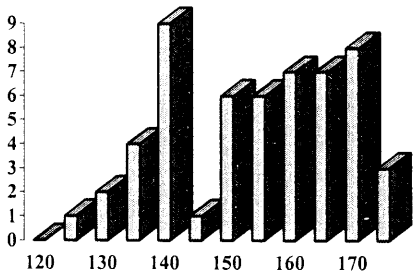

Fig. 15. Histogram of the scattering angles observed on 50 SeaWiFS images for a 2-year period over the Venice site.

50 SeaWiFS images for a 2-year period over the Venice site (see Fig. 15). In 60% of the cases the scattering angles are superior to 140°. We have approximately 50 SeaWiFS images per year in coincidence with the CIMEL measurements. We can use half of the images due to the restriction of the geometrical conditions. Four years of SeaWiFS data are available. For the Venice site we have approximately 100 points to lead the calibration–validation activity, which is enough. If we use the AERONET data, we have much more data to process.

4. Conclusion

Through use of the spectral dependency of the aerosol optical thickness we have shown that the SeaWiFS TOA reflectance retrieved was not accurate enough. To conduct this work, knowledge of the aerosol model is less relevant than knowledge of the phase function. We illustrated this point on one data set by using the Dubovik and King[13] method to get the aerosol model. The inverted aerosol model does not allow the retrieval of the sky radiance in backscattering where we need an accurate estimate to evaluate the satellite signal.

We have presented then a method for inverting the non-normalized phase function P_a or P by using *in situ* measurements from the principal plane. Our inversion is based on application of the single-scattering approximation to CIMEL PPL radiance measurements previously decontaminated from the multiple-scattering effects. This correction from multiple scattering was done with the primary to multiple-scattering ratio f. Because f does not depend much on the aerosol model, this method is accurate and converges very fast. The accuracy of the phase function retrieval has been estimated to be better than 1% if all the other parameters are known. The precision is slightly degraded below 1% with uncertainty about the wind speed accounting for the Fresnel reflection as boundary conditions. Other parameters, barometric pressure, relative vertical distribution, may also bias the phase-function retrieval, but the effect on the TOA signal estimate remains negligible. From a practical point of view, we have the following limitations:

(i) An error in the calibration of the CIMEL instrument leads to the same relative error in the TOA radiances.

(ii) CIMEL measurements at the same scattering angle as satellite observation never occur at the time of overpass: Phase functions derived in the early morning are used at noon, and, even if we can monitor the stability of the atmosphere, an additional error of the order of 1% is predictable on stable days.

(iii) Because we have no access from the ground to scattering angles greater than 140°, the number of useful space observations is limited. To counterbalance this, it was useful to develop this technique for a network of radiometers. Our method may be more easily applied to the assessment of TOA reflectances measured by the moderate-resolution imaging spectrometer (MODIS) and MERIS, for which the scattering angles will be lower owing to the hour of overpass (10:30 a.m. instead of noon for SeaWiFS) as well as the viewing conditions (no tilt avoids the glitter contribution contrary to SeaWiFS).

We can also apply the same methodology to the almulcantar. The scattering angle range is limited except for the first data set collected at an air mass equal to 5 ($\Theta = 157°$). We can also blame the scanning protocol. The CIMEL instrument aims mainly at the optical characterization of the aerosols based on interpretation of the forward scattering. As a consequence the view angular step scan for the PPL protocol measurements is only 10° when the scattering angles are greater than 70°. Adapting the step scan to the CIMEL PPL protocol with a narrow angular step should be useful.

The proposed method can be used to lead a vicarious calibration of ocean-color sensors in the near IR, which is interesting when one considers the problems of the temporal degradation of bands 7 and 8 of SeaWiFS.[4] The method can also be employed to make atmospheric corrections in the visible bands, a crucial point for the satellite sensors over coastal waters, where negative water-leaving radiances are usually observed. We need to completely validate the method at 443 nm through the use of an important set of ground-based data. Indeed the CIMEL data are used throughout the AERONET network.

Finally, even if assessment of the TOA reflectances needs only the atmospheric phase function, P_a can also be derived and interpreted. Indeed aerosols encountered over coastal waters are complex, and the standard climatology defined by Shettle and Fenn in the SeaWiFS algorithm is no longer adaptable. The aerosol phase function as well as other *in situ* aerosol products could allow the optical characterization of the aerosols in the frame of local aerosol climatology, in order to improve SeaWiFS atmospheric corrections in coastal areas.

This study was realized because of data acquired from the framework of the Colors project. We mainly thank G. Zibordi for access to the CIMEL measurements performed at the Venice tower. We also thank Frédéric Lemire, Xavier Mériaux, and Olivier Hars for their technical help.

References

1. H. R. Gordon, "Calibration requirements and methodology for remote sensors viewing the ocean in the visible," Remote Sens. Environ. **22,** 103–126 (1987).
2. R. A. Barnes and R. E. Eplee, Jr., "The SeaWiFS solar diffuser," in *SeaWiFS Calibration Topics, Part 1*, NASA Tech. Memo. 104566, **39,** R. A. Barnes, E-N. Yeh, and R. E. Eplee, Jr., eds. (NASA Goddard Space Flight Center, Greenbelt, Md., 1996).
3. H. H. Kieffer and R. L. Widley, "Establishing the moon as a spectral radiance standard," J. Atmos. Ocean. Technol. **13,** 360–375 (1996).
4. R. A. Barnes, R. E. Eplee, Jr., F. S. Patt, and C. R. McClain, "Changes in the radiometric sensitivity of SeaWiFS determined from lunar and solar-based measurements," Appl. Opt. **38,** 4649–4664 (1999).
5. M. Wang and B. Franz, "Comparing the ocean color measurements between MOS and SeaWiFS: a vicarious intercalibration approach for MOS," IEEE Trans. Geosci. Remote Sens. **38,** 184–197 (2000).
6. H. R. Gordon and T. Zhang, "How well can radiance reflected from the ocean–atmosphere system be predicted from measurements at the sea surface?" Appl. Opt. **35,** 6527–6543 (1996).
7. B. Holbén, T. Eck, I. Slutsker, D. Tanré, J. P. Buis, A. Setzer, E. Vermote, J. Reagan, Y. Kaufman, T. Nakajima, F. Lavenu, I. Jankowiak, and A. Smirnov, "AERONET—a federated instrument network and data archive for aerosol characterization," Remote Sens. Environ. **66,** 1–16 (1998).
8. H. R. Gordon and M. Wang, "Retrieval of water-leaving radiances and aerosol optical thickness over the oceans with SeaWiFS: a preliminary algorithm," Appl. Opt. **33,** 443–452 (1994).
9. J. L. Deuzé, M. Herman, and R. Santer, "Fourier series expansion of the transfer equation in the atmosphere–ocean system," J. Quant. Spectrosc. Radiat. Transfer **41,** 483–494 (1989).
10. R. Santer and M. Herman, "Particle size distributions from forward scattered light using the Chahine inversion scheme," Appl. Opt. **22,** 2294–2301 (1983).
11. T. Nakajima, M. Tanaka, and T. Yamauchi, "Retrieval of the

optical properties of aerosols from aureole and extinction data," Appl. Opt. **22,** 2951–2959 (1983).
12. M. Wang and H. R. Gordon, "Retrieval of the columnar aerosol phase function and single scattering albedo from sky radiance over the ocean: simulations," Appl. Opt. **32,** 4598–4609 (1993).
13. O. Dubovik and M. King, "A flexible inversion algorithm for retrieval of aerosol optical properties from Sun and sky radiance measurements," J. Geophys. Res. **105,** (ND16), 20,673–20,696 2000.
14. C. Devaux, A. Vermeulen, J. L. Deuzé, P. Dubuisson, M. Herman, and R. Santer, "Retrieval of aerosol single scattering albedo from ground-based measurements: application to observational data," J. Geophys. Res. **103,** 8753–8761 (1998).
15. E. P. Shettle and R. W. Fenn, "Models of the aerosols of the lower atmosphere and the effects of humidity variations on their optical properties," Technical Report 0214 (Air Force Geophysical Laboratory, Hanscom Air Force Base, Mass., 1979).
16. D. Tanré, C. Deroo, P. Duhaut, M. Herman, J. Morcrette, J. Perbos, and P. Y. Deschamps, "Description of a computer code to simulate the satellite signal in the solar spectrum: 5S code," Int. J. Remote Sens. **11,** 659–668 (1990).
17. N. Martiny and R. Santer, "Atmospheric corrections over coastal waters for SeaWiFS: validation using ground-based measurements," in *Ocean Optics: Remote Sensing and Underwater Imaging*, G. D. Gilbert and R. J. Frouin, eds., Proc. SPIE **4488,** 184–194 (2002).